World Academy of Science, Engineering and Technology
International Journal of Materials and Metallurgical Engineering
Vol:12, No:3, 2018

SEM-EBSD Observation for Microtubes by Using Dieless Drawing Process

Takashi Sakai, Itaru Kumisawa

***Abstract*—**Because die drawing requires insertion of a die, a plug, or a mandrel, higher precision and efficiency are demanded for drawing equipment for a tube having smaller diameter. Manufacturing of such tubes is also accompanied by problems such as cracking and fracture. We specifically examine dieless drawing, which is less affected by these drawing-related difficulties. This deformation process is governed by a similar principle to that of reduction in diameter when pulling a heated glass tube. We conducted dieless drawing of SUS304 stainless steel microtubes under various conditions with three factor parameters of heating temperature, area reduction, and drawing speed. We used SEM-EBSD to observe the processing condition effects on microstructural elements. As the result of this study, crystallographic orientation of microtube is clear by using SEM-EBSD analysis.

***Keywords*—**Microtube, dieless drawing, IPF, inverse pole figure, GOS, grain orientation spread, crystallographic analysis.

I. Introduction

THERE are a lot of methods to product the microtube. Furushima et al. performed reduction in the diameter of a microtube dieless drawing using local heating and tension [1], [2]. However, further diameter reduction has been prevented by cracking and fracture. Enhancement of the ratio of the grain diameter to the dimension of raw materials because of down-scaling encourages a closer relation between material properties and crystallographic characteristics [3]. Such down-scaling is necessary to manufacture high-precision tubing to study the variation of microscopic properties, such as texture and crystallographic orientation of materials by deformation. This study was conducted to elucidate the effects of heat and tension accompanying dieless drawing and to assess the influence of a drawing process on texture, in terms of crystallographic orientation as a microscopic material property.

II. Experimental

A. Test Specimens

This study used SUS304 austenitic stainless-steel tubes with respective initial outer and inner diameters of 500 μm and 240 μm.

B. Dieless Drawing

Fig. 1 presents a schematic diagram of the dieless drawing process. Dieless drawing achieves the areal reduction of a cross-section of a tube by imparting heating and tensile deformation locally. It is not using any tools for drawing such as a die. Drawing speed V_1 in excess of the feeding speed V_2 produces tension. The areal reduction of a tube R by drawing can be expressed with V_1 and V_2 by the constant volume principle as expressed in (1). Total reduction of area R_t by multi-pass drawing of two or more times combined with dieless drawing can be expressed as (2).

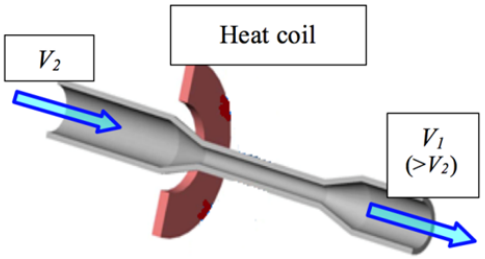

Fig. 1 Schematic illustration of dieless drawing

TABLE
Conditions of Dieless Drawing

(As-received (1))			Area reduction R /%			
			0	20	30	40
Heating temperature T /℃	1 Pass	850	(2)	(4)	(10)	–
		900	–	(5)	(11)	(16)
		950	–	(6)	(12)	(17)
		1000	(3)	(7)	(13)	(18)
		1100	–	(8)	(14)	–
		1200	–	(9)	(15)	–
	Multi-pass	950	0+44.4 (19)			
			20+32.4 (20)			
			0+20+31.9 (21)			
		1000	20+40 (22)			
			30+30 (23)			

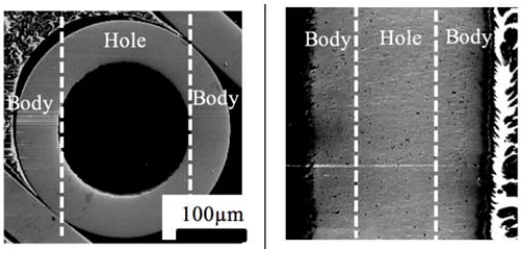

(a) Cross sectional direction (b) Longitudinal direction

Fig. 2 SEM images of the imitional tube

$$R = 1 - V_2/V_1 \quad (1)$$

$$R_t = 1 - (1 - R_1)(1 - R_2)\cdots(1 - R_n) \quad (2)$$

Takashi Sakai is with the Faculty of Science and Engineering, Seikei University, Tokyo 180-8633, Japan (phone and fax: +81-422-37-3712; e-mail: sakai@st.seikei.ac.jp).
Itaru Kumisawa is with the master course of Science and Engineering, Seikei University, Tokyo 180-8633, Japan (phone: +81-422-37-3719).

Table I presents the dieless drawing conditions. In all, 23 tube specimens were prepared for this study: (1) as-received; (2)-(18) processed with reduction of area *R*, with heating temperature *T* varied; and (19)-(23) processed by multi-pass drawing. Specimens at low and high temperature regions fracture before completion of reduction in drawing at *R*=40%.

C. Polishing and Observation of Samples

Samples subjected to electron backscatter diffraction (EBSD) measurement were prepared by surface polishing with emery paper (#2000) and Al_2O_3 abrasives of 1.0 μm, 0.3 μm, and 0.05 μm for 600 s for each step. Then, electrolytic polishing was performed as final polishing for the measured samples, using a mixture solution of CH_3OH:$C_6H_{14}O_2$:$HClO_4$ of a proportion of 5:3:1 with a Pt counter electrode at 30V and 3A for 3 s. Crystallographic orientation was measured using EBSD with FE-SEM. Various crystal orientation analyses were conducted with software (OIM ver.6.0; TSL Solutions, Inc.).

Fig. 2 portrays SEM images of the obtained tubes, where panels (a) and (b) respectively show a cross section image and a longitudinal section image. EBSD measurement points were chosen from the wall part on the longitudinal section (body section in Fig. 2 (b)). Measurements were taken at a constant magnification of 1,500 so that a sufficient number of grains were measured for analyses, with 3μm step size.

III. Experimental Results and Discussion

A. Areal Reduction

Table II presents the measurement results of the areal reduction. The longitudinal section of a tube processed according to each experimental condition was polished. The inner and outer diameters were ascertained from the SEM image. Then a boss ratio and true reduction of area were computed and compared with those of the as-received raw tube.

TABLE II
List of Area Reduction

Area reduction (%)	Heat temp (℃)	Outer diameter (μm)	Inner diameter (μm)	Inner/outer diameter ratio	Real area Reduction (%)
As-received		488.7	301.2	0.62	0
20	(4) 850	426.9	256.6	0.61	23.7
	(5) 900	418.4	248.7	0.60	26.7
	(6) 950	430.7	261.6	0.61	22.3
	(7) 1000	436.5	264.3	0.61	20.2
	(8) 1100	445.3	198.3	0.45	16.9
	(9) 1200	436.2	261.9	0.60	20.3
30	(11) 900	410.7	245.5	0.60	29.3
	(12) 950	404.6	242.6	0.60	31.5
	(13) 1000	414.8	247.9	0.60	28.0
	(14) 1100	403.7	243.8	0.60	31.7
	(15) 1200	415.3	259.2	0.62	27.8
40	(16) 900	390.2	190.1	0.49	36.2
	(17) 950	387.9	205.7	0.53	37.0
	(18) 1000	375.4	227.1	0.60	41.0

The boss ratio of the as-received raw tube was 0.62. This value remained almost constant at *R*=20, 30, and 40%, which suggests that a fixed boss ratio is always obtained by dieless drawing. The theoretical and experimental values of the total reduction of area generally agreed. However, some errors were found for specimens (8) and (16), probably because temperature deviation of about ±50 °C in the heating apparatus of the laboratory equipment caused a difference in deformation resistance. Consequently, a fixed boss ratio, high areal reduction, and a beautiful inner surface were demonstrated by dieless drawing.

TABLE III
Behavior of Re-Crystallization

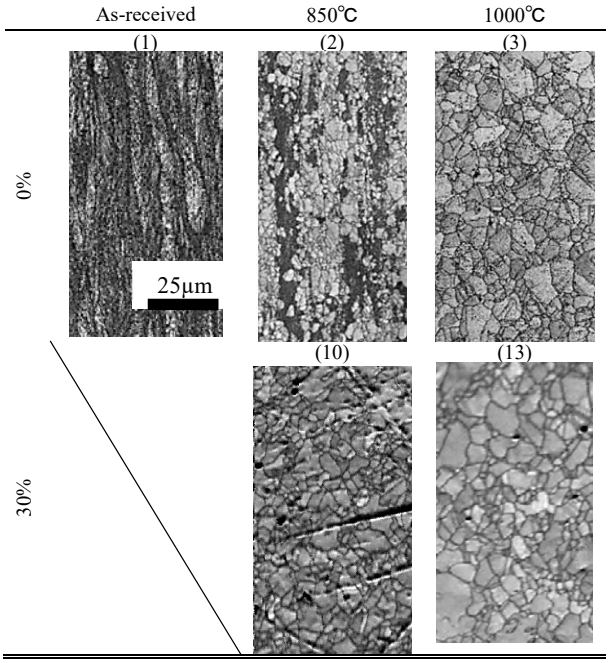

B. Recrystallization Behavior

Table III presents image quality (IQ) maps of the following: (1) and (2) as-received; (3) tubes with *R*=0%, and (10) and (13) tubes with *R*=30%. The IQ map shows the diffraction intensity of the Kikuchi pattern, and corresponds to crystal conformation. The intensity tends to decrease (the map turns black) when the crystal structure is distorted by plastic deformation, such as that from mechanical processing, although it tends to increase (white) when free from strain [4].

The as-received tube presented crystals elongated in the longitudinal direction in an indistinct IQ map because of a bad crystal state with concentrated strain. Because the as-received tube was manufactured by die drawing, high strain had affected the material.

Specimen (2) showed partial but mostly incomplete recrystallization, suggesting that it was still in its early stage, whereas recrystallization was completed in specimen (10), subjected to 30% drawing at the same temperature. Consequently, recrystallization occurred in specimens with strain imparted by dieless drawing at lower temperatures compared to specimens with no reduction. Recrystallized grains were observed over the whole specimen (3) heated at 1000 °C.

The recrystallization temperature of SUS304 is around 700–750 °C. However, recrystallization took place at temperatures higher than the intrinsic recrystallization temperature in dieless drawn materials because of the extremely short heating time.

C. Measurement Results of One-Pass Drawn Material

The EBSD measurement results of one-pass drawn specimens in Table IV present inverse pole figure (IPF) maps at various temperatures for R=20%, along with the analysis result on low and high angle grain boundaries. The IPF maps indicated considerable variation in neither diameter nor orientation of grains up to 950 °C and 1100 °C, but grain coarsening took place at 1,200 °C.

The analysis of low-angle and high-angle grain boundaries revealed that low-angle boundaries as a deformed structure prevailed at 900 °C or lower temperatures, but decrease in low-angle boundaries was observed at 950 °C. The fraction of low-angle boundaries disappeared gradually with temperatures rising to 1,100 °C and 1,200 °C. This result suggests completion of recrystallization at 950 °C or higher temperatures.

Relaxation of a deformed structure in a grain improves workability, whereas coarse grains by grain growth deteriorate workability. Fig. 3 is a chart representing the relation between the critical reduction of area and heating temperature. The areal reduction is maximal at around 950–1100 °C; it tends to decrease gradually with temperatures higher than the peak temperature. This result agrees with the hypothesis of improved workability by a decrease in low angle grain boundaries and a decline in workability by grain growth, as shown in Table IV. Consequently, the optimal heating temperature in one-pass drawing is found to be around 950–1100 °C.

TABLE IV
IPF MAPS AND HIGH- AND LOW-ANGLE BOUNDARY FOR 1PASS

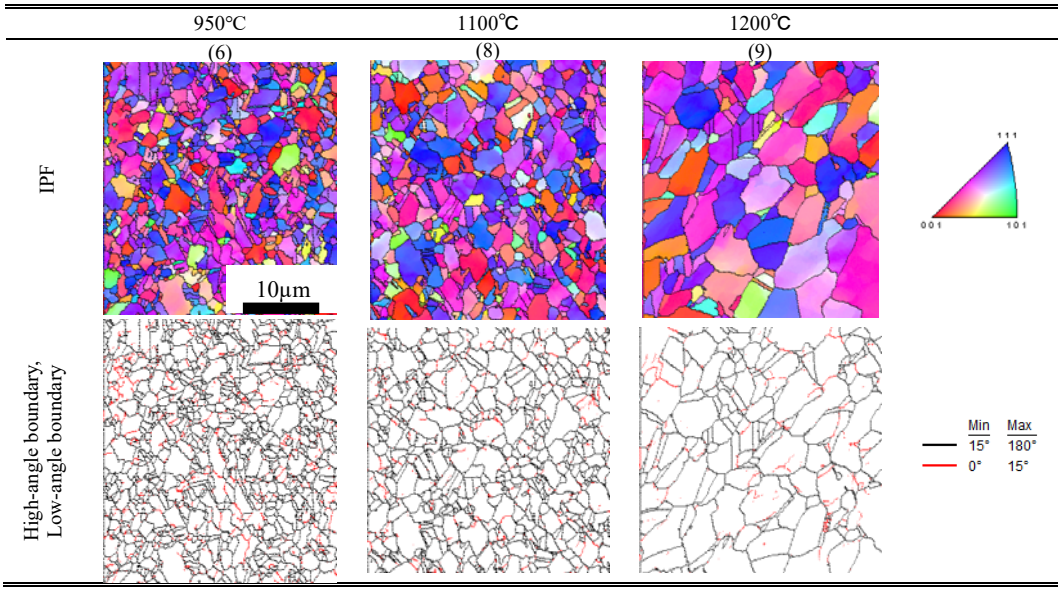

TABLE V
IPF AND GOS MAPS FOR MULTI PASS

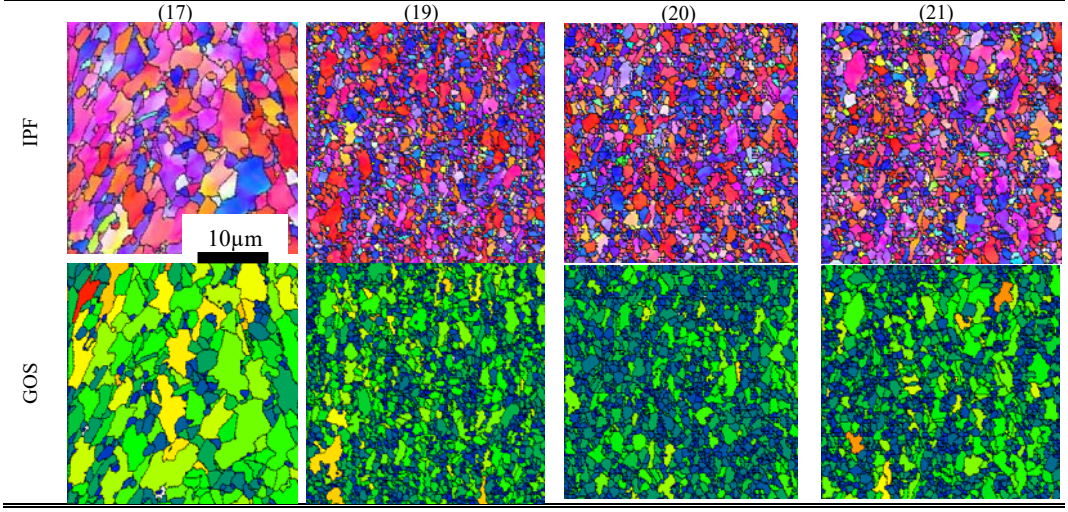

D. Measurement Results of Multi-Pass Drawn Tubes

Table V presents analysis results of the IPF map and a Grain Orientation Spread (GOS [5]) map of multi-pass drawn tubes. Effects of drawing schedules was observed when test pieces were dieless-drawn to fracture at a heating temperature fixed at 950 °C considering the result of the one-pass experiments.

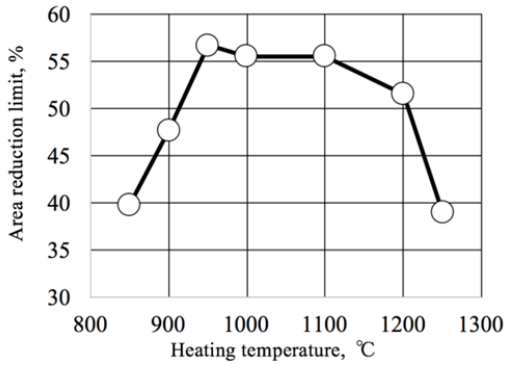

Fig. 3 Relationships between heat temperature and area reduction limit

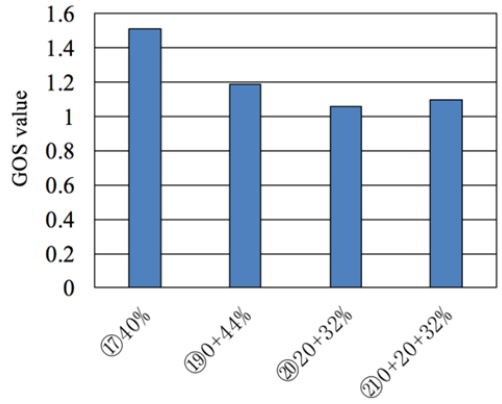

Fig. 4 GOS value for different drawing passes

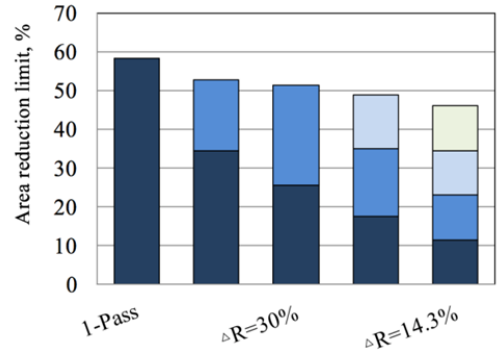

Fig. 5 Relationships between drawing cycle and area reduction limit

The IPF map indicated no difference for specimens (19), (20), and (21). The total reductions of area were 44.4%, 45.9%, and 45.5%, respectively, for specimens (19), (20), and (21) so that no big difference was observed either.

Fig. 4 shows the quantitative chart of GOS values computed from the GOS maps. Although a one-pass drawn specimen (1) had a high value, no large difference was found in multi-pass drawn specimens (19)-(21). These results suggest that differences in a drawing schedule do not affect the total reduction of the area and microscopic factors.

The relation between the critical reduction of area and the number of drawing passes is presented in Fig. 5, which indicates that an increase in the number of drawing passes tends to degrade the critical reduction of area. We infer that this is true because the surface roughness is enhanced as the number of drawing passes increases. When the number of drawing passes is increased, surface roughness also increases, so that the area reduction decreases. It is presumed that even a little surface roughness of a microtube might easily cause fracture because of its very thin walls.

Consequently, it is difficult to apply the present multi-pass drawing technique for manufacturing of microtubes. However, reduction of surface roughness by polishing, etc., after each pass might further reduce the tube diameter by multi-pass drawing.

IV. Conclusions

Microtubes manufactured using dieless drawing were subjected to SEM-EBSD measurement. The following results were obtained.

1. Examination of the reduction of area revealed that the inner diameter was sustained without using a die, that excellent reduction of area close to the theoretical value was attained, and that the boss ratio was always constant.
2. Examination of recrystallization behavior verified recrystallization at low temperatures in cases where strain was introduced by dieless drawing. However, very short heating time prevented recrystallization at 700–750 °C. This is the intrinsic recrystallization temperature of SUS304.
3. One-pass drawing experiment results indicated many low-angle grain boundaries as a deformation structure remaining to a certain temperature and gradual annihilation with rising temperatures.
4. Multi-pass drawing experiment results revealed that differences in the drawing schedule did not affect microscopic factors.
5. Multi-pass drawing experiment results also revealed that an increased the number of drawing passes led to a decline in the critical reduction of area. Presumably, this is true because enhanced surface roughness accompanies an increase in the number of drawing passes.

References

[1] T. Furushima, K. Manabe and T. Sakai, "Fabrication of Superplastic Microtubes Using Dieless Drawing Process (Periodical style)", *Journal of the JSTP*, Vol. 47, No. 548, 2006, pp. 870-874.

[2] T. Furushima and K. Manabe, "Fabrication of AZ31 Magnesium Alloy Fine Tubes by Dieless Drawing Process (Periodical style)", *Journal of the JSTP*, Vol. 51, No. 597, 2010, pp. 990-992.

[3] S. Biswas, S. Suwas, R. Sikand and A. K. Gupta, "Analysis of texture evolution in pure magnesium and the magnesium alloy AM30 during rod and tube extrusion (Periodical style)", *Materials Science and Engineering*, Vol. A-528, 2011, pp. 3722-3729.

[4] M. Kamaya, "Measurement of Plastic Strain Distribution by Electron Backscatter Diffraction (Periodical style)", *Journal of the Society of*

Materials Science Japan, Vol. 58, No. 7, 2009, pp. 568-574.

[5] H. Kimura, Y. Wang, Y. Akiniwa and K. Tanaka, "Misorientation Analysis of Plastic Deformation of Austenitic Stainless Steel by EBSD and X-Ray Diffraction Methods (Periodical style)", *Transactions of the JSME*, Vol. 71, No. 712, 2005, pp. 1722-1728.